International Journal of Design & Nature and Ecodynamics
Vol. 18, No. 1, February, 2023, pp. 11-20
Journal homepage: http://iieta.org/journals/ijdne

# Sugarcane Bagasse-Derived Cellulose as an Eco-Friendly Adsorbent for Azo Dye Removal

Haya Fathana[1], Rahmi[2*], Muhammad Adlim[1,3], Surya Lubis[2], Muhammad Iqhrammullah[4]

[1] Graduate School of Mathematics and Applied Sciences, Universitas Syiah Kuala, Kopelma Darussalam, Banda Aceh 23111, Indonesia
[2] Department of Chemistry, Faculty of Mathematics and Natural Sciences, Universitas Syiah Kuala, Kopelma Darussalam, Banda Aceh 23111, Indonesia
[3] Department of Chemistry Education, Faculty of Teacher Training and Education, Universitas Syiah Kuala, Banda Aceh 23111, Indonesia
[4] Innovative Sustainability Lab, PT. Biham Riset dan Edukasi, Banda Aceh 23243, Indonesia

Corresponding Author Email: rahmi@fmipa.unsyiah.ac.id

https://doi.org/10.18280/ijdne.180102

**Received:** 20 December 2022
**Accepted:** 10 February 2023

***Keywords:***
*cellulose particles, sugarcane bagasse, adsorption, methylene blue*

**ABSTRACT**

Cellulose has been isolated from sugarcane bagasse and applied for azo dye adsorption. Hydrolysis process for cellulose isolation was performed with different concentrations of HCl and the best concentration was 20% (v/v). Fourier Transform Infrared Spectroscopy (FTIR), X-ray Diffraction (XRD), and Thermogravimetric Analysis (TGA). The increase in peak intensity at wavenumber 897 $cm^{-1}$ was connected to cellulose stretching C-O and C-H, which resulted in greater cellulose content following hydrolysis. The thermal resistance of cellulose enhanced after treatments due to the significant intermolecular hydrogen bonding in the cellulose particles. Cellulose particles have been studied for their capacity to eliminate methylene blue (MB) from aqueous solutions. The analysis indicated that the OH, C=O, and C-O groups were particularly important in azo dye adsorption based on FTIR data. After 120 minutes of methylene blue adsorption and adsorption conditions at pH 10, a very high percent removal was obtained, precisely 99.7%. Based on adsorption kinetics, MB adsorption adopted a pseudo-second-order model (PSO) with an adsorption rate constant ($k_2$) was 0.0276 g/mg.min. According to isotherm investigations, Freundlich isotherm model dependent adsorption (adjusted-$R^2$ =0.928), with Kf = 66.386 mg/g.

## 1. INTRODUCTION

An important agricultural crop, sugarcane is cultivated in tropical and subtropical areas all over the world. Sugarcane has long been acknowledged to be one of the most effective crops at turning solar energy into chemical energy, which can be collected as sucrose and biomass [1]. After its production from the fields, sugarcane was brought to the manufactory and used to extract juice from sugar production. Sugarcane cultivation contributes to roughly 80% of world sugar demand [2]. The sugarcane sector was important for tropical and subtropical nations not only for sugar production, which is a key export product for many emerging economies but also for its byproducts. More than 50 first-generation and over 100 second-generation products may be made from byproducts of the sugarcane and agricultural industries. Sugarcane by-products are used as raw materials to make paper pulp, plywood, animal feed, wax, biofertilizers, alcohols, and many other valuable goods [3]. Sugarcane bagasse is significant by-product of industrial sugarcane processing [4]. It is typically produced following cleaning and extraction of sugarcane juice. Sugarcane bagasse (SCB) is a fibrous residue that contains approximately 17-32% lignin, 20-32% hemicellulose, 1.0-9.0% ash, 32-45% cellulose, and other components [5].

Cellulose is a common natural polymer produced from several materials, such as wood, plants, and microbes [6]. Because of their sustainability and renewability, cellulosic materials are gaining popularity as biocomposites agents for medical and industrial applications. They have many of (-OH) groups on their surfaces, which are chemically malleable. They have excellent mechanical qualities, a low toxicity, a high aspect ratio, and a low density [6, 7].

Various pre-treatment techniques have been developed to remove hemicellulose, lignin, wax, ash, and other non-cellulosic substances from plant cellulose [8]. These cellulose materials are instinctive formed into cellulose nanocrystals (CNC), cellulose nanofibrils (CNF), cellulose nanoparticles (CNP), and bacterial nanocellulose (BNC) through chemical or mechanical pre-treatment [9]. The dewaxing process was started with the purpose of removing the wax content contained in the SCB. Fatty deposits, aldehydes, fatty acids, esters, and hydrocarbons were discovered in wax [10]. Some researchers that separate cellulose from natural sources still rarely use this method. The fact that this approach reduced the wax component in the SCB by about 94% [11]. Considering how important the dewax process is and the researchers rarely do this step first, in this study the dewax process was carried out first before proceeding to the alkalization and hydrolysis steps. In order to reduce the amount of lignin and make it

easier to separate the cellulose, the SCB's lignocellulosic structure was then disrupted during the alkalization process [12]. This is followed by an acid-based hydrolysis. The hydrolysis of cellulose with acid, which dissolve amorphous cellulose to produce well-defined crystalline domains. Acid hydrolysis successfully dissolves amorphous cellulose and extracts CNC from it [13, 14]. Some researchers have been used $H_2SO_4$ for hydrolysis of cellulose [3, 15, 16]. This is a consideration in this study because $H_2SO_4$ has hygroscopic properties. So in this study, the process of hydrolysis using HCl. To establish the optimal concentration, the hydrolysis process was carried out in this investigation utilising HCl solutions at concentrations of 5, 10, 20, 25, and 30%. Acid hydrolysis is used to break down cellulose, and cellulose is then produced by separating the crystalline domains from the amorphous component [17]. The properties of cellulose particles were also evaluated based on the characterization results using FTIR, XRD, and TGA.

In this study, cellulose particles were used to methylene blue (MB) adsorption. Methylene blue is a cationic azo dye produced in textile industry waste, which pollutes the aquatic environment. Methylene blue consumption has been proven in studies to have negative effects on human health, including symptoms such as vomiting, irregular heartbeat, excessive sweating, gastritis, and chest discomfort [18]. As a result, an effective and efficient approach for removing MB from industrial effluent is required. Because of its ability to remove cationic dyes, the cellulose derived from sugarcane bagasse is a particularly beneficial product for the environment. Naturally, this is one of the reasons we wanted to change SCB, a useless product at first, into a highly useful product. Herein, we also studied how methylene blue adsorbs to cellulose, focusing on the effects of contact time, pH, adsorption kinetics, and adsorption isotherms. The findings of this study, there was an increase in α-cellulose composition as well as an increase in HCl concentration during the hydrolysis process. The maximum crystallinity index, 63.57%, was found at a concentration of 20% HCl. The optimal conditions for methylene blue adsorption using cellulose were 120 minutes and pH 10. Isothermal studies have shown that this adsorption process follows the Freundlich isotherm model. The structure of this paper includes an introduction, materials and methods, results and discussion, and conclusions. In this paper we discuss cellulose isolation, evaluation of cellulose composition, characterization, and adsorption studies of methylene blue in the materials and methods sections as well as results and discussion.

## 2. MATERIALS AND METHODS

### 2.1 Materials

This study's materials included HCl, NaOH, toluene, ethanol, distilled water, 15% $NaClO_2$, Methylene Blue, and SCB (collected solid waste from a supplier of sugarcane juice drinks in Banda Aceh, Indonesia). All of the compounds were analytical grade and acquired from Sigma-Aldrich (Selangor, Malaysia).

### 2.2 Cellulose particles isolation

*a. Preparation*

Herbarium testing was used to identify SCB species. SCB was cleaned and dried until no water remained. The SCB was then chopped into little pieces. Using a pestle and mortar, the sugarcane bagasse was pounded to a powder of around 0.5 mm. After processing, SCB was stored in a ziplock bag for later use.

*b. Dewaxing process*

A magnetic stirrer was used to stir SCB in a 2:1 mixture of toluene and ethanol for 24 hours at room temperature. The mixture was then filtered and steeped in distilled water until it achieved a pH of 7. Following that, filtration using a Buchner funnel and vacuum was undertaken, followed by 20 hours of drying in a 50℃ oven.

*c. Alkalization process*

Sample was soaked in 5% NaOH and stirred for 4 hours at 50℃ with a magnetic stirrer at 500 rpm. After that, the suspension was filtered through a Buchner funnel and diluted with distilled water until pH 7. The sample was then heated in a 50℃ oven for 20 hours before being weighed [19].

*d. Hydrolysis process*

The procedure employed in this section was the same as that used by Abral et al. [19], with the exception of minor changes in HCl concentration variations. SCB was hydrolyzed at 50℃ for 12 h at HCl concentrations of 5, 10, 20, 25 and 30%. After filtering and vacuuming the hydrolyzed cellulose, it was rinsed with distilled water until the pH reached neutral. It was then dried in a 50℃ oven for 20 hours.

e. *Bleaching process*

The hydrolyzed cellulose was immersed in a 4:1 solution of NaOCl and $CH_3COOH$ and swirled with a magnetic stirrer for two hours at a speed of 500 rpm and a temperature of 60℃. After bleaching the cellulose, it was washed with distilled water until the pH was neutral [19].

*f. Ultrasonications process*

Ultrasonication was performed with a 600 W voltage ultrasonic. At a maximum temperature of 60℃, 100 mL of suspension was sonicated for 60 minutes.

### 2.3 Evaluation of cellulose particle composition

The ASTM D5896-96 technique was used to determine the hemicellulose content [20]. 10 mL of 0.5 M NaOH was mixed with 1 g of sample. It was placed in a 100℃ boiling water bath for 3 hours before being rinsed and filtered with distilled water. After that, it was dried in a 50℃ oven for 12 hours. Eq. (1) is used to determine the results based on a method in the literature [20].

$$\text{The presence of hemicellulose} = W_i - W_f \quad (1)$$

where, $W_i$ and $W_f$ are the starting weight and the final weight respectively.

1 g of the material was mixed with 72% $H_2SO_4$ while stirring to determine the lignin concentration. Following that, the sample was let to stand for 1 hour until being diluted with $H_2SO_4$ 3% and placed in a water bath at 100℃ for 4 hours. The filter paper was measured and weighed. The material was then filtered, neutralised, and dried for 12 hours at 50℃. Furthermore, the lignin content of the sample and filter paper was determined using Eq. (2) based on a method in the literature [20].

$$\text{The presence of lignin (\%)} = \frac{W_d}{W_i} \text{ x } 100 \quad (2)$$

$W_d$, $W_i$ are the dried sample's weight and the starting weight respectively. The cellulose content was determined by Eq. (3) based on a method in the literature [20].

$$Cellulose\ \% = 100 - (Hemicellulose + lignin) \quad (3)$$

### 2.4 Characterization

To study functional groups, samples were cleaved on sample holders and oven-dried overnight at 40℃ prior to Fourier transform infrared (FT-IR) analysis. The functional groups were identified using the Shimadzu FT-IR 8400 (Kyoto, Japan). The analysis was carried out in the 4000-400 $cm^{-1}$ range. The samples which were characterized using FT-IR were cellulose particles before hydrolysis, cellulose particles after hydrolysis using HCl 5, 10, 20, 25 and 30%. Peak and intensity alterations were observed in all samples. Shimadzu XRD-700 Series X-Ray Diffractometer was used for crystal structure analysis (Kyoto, Japan). Cu $K\alpha_{1,2}$ radiation (1.54060 nm) was used to scan the samples from 10° to 30° (2θ), at a speed of 8/min. The X-ray generator's tube current was 30 mA and it ran at 40 kV. The samples which were characterized using XRD were SCB (row material), cellulose (in powder) before hydrolysis, cellulose after hydrolysis using HCl 5, 10, 20, 25 and 30%. Thermal characteristics of the sample were examined using thermal gravimetry analysis (TGA), in which the sample (1 mg) was placed on an aluminium cell and heated from 50 to 600℃ at a rate of 40 C/min in a Shimadzu DTG-60 Thermal Gravimetric Analyzer in a dynamic nitrogen atmosphere (flow rate: 20 mL/min) (Kyoto, Japan).

### 2.5 Adsorption study

*a. Parameters of adsorption*

There were two value parameters, the contact time and pH of solutions. 0.5 g of cellulose particles were added to 20 mL of 20 mg/L methylene blue solution in 250 mL Erlenmeyer. The mixture was then shaken with varying contact times (10, 50, 80, 120 and 180 minutes). After filtering methylene blue, a UV-Vis spectrophotometer (UVmini1240, Shimadzu Corporation, Kyoto, Japan) was used to measure its absorbance at its maximum wavelength. Next, pH of methylene blue (pH 2-10) was varied to investigate the effect of pH by adding 0.1 M HCl and 0.1 M NaOH. Eqns. (4) and (5) were used to provide the data as equilibrium adsorption volume (Qe (mg/g)) and percent removal (%) according to reference [21].

$$Qe = \frac{C_o - C_e}{W_x} . V_y \quad (4)$$

$$\%R = \frac{C_o - C_e}{C_o} \text{ x } 100 \quad (5)$$

$C_e$, $C_o$, $V_y$ and $W_x$ are equilibrium concentration (g/ml), the initial concentration (g/ml), volume of adsorbate (ml), and weight of adsorbent (g), respectively.

In addition to the effect of pH, we also calculated the $pH_{pzc}$ of the adsorbent. The $pH_{pzc}$ was determined using the pH drift method with 0.1 M $KNO_3$ above a contact duration of 72 hours [22].

*b. Adsorption isotherm*

The maximum adsorption capacity of cellulose was determined via an equilibrium isotherm analysis. The isotherm was established by varying the MB concentration. The concentrations used in this investigation were 10, 20, 30, 40, and 50 mg/L with 0.5 g of cellulose particles.

*c. Adsorption kinetic*

Adsorption kinetics describes the rate of adsorption of the adsorbent to the adsorbate. By analyzing MB concentrations at each time of contact (10, 30, 50, 80, 120, and 180 minutes) with 0.1 g of cellulose, the adsorption kinetics model of MB by cellulose was established. To determine the mechanism of adsorption, the experimental data was fitted with pseudo first order (PFO) (6) and pseudo second order (PSO) (7) kinetic models according to reference [23].

$$q_t = q_m(1 - e^{k_1 t}) \quad (6)$$

$$q_t = \frac{q_m^2 k_2 t}{1 + q_t k_2 t} \quad (7)$$

## 3. RESULTS AND DISCUSSIONS

SCB utilised in this study was identified by herbarium investigation at the Faculty of Mathematics and Natural Sciences, Universitas Syiah Kuala (voucher number. 20/UN11.1.8.4/TA.00.01/2022). According to the findings, the SCB used in this study was Saccharum officinarum Linn.

### 3.1 Cellulose particles isolation

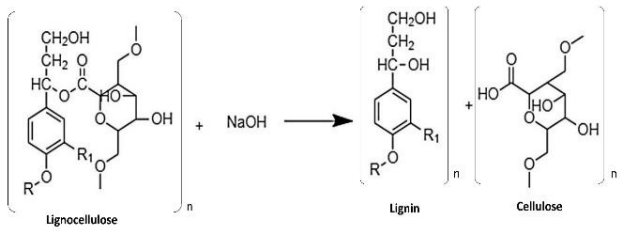


**Figure 1.** The mechanism of lignin-cellulose bond dissociation in lignocellulose using NaOH

This step begins with the dewaxing treatment. It sought to remove the wax components of the SCB. 80% of the extracted material was recovered by this procedure. The most popular approach for removing lignin and hemicelluloses from lignocellulosic materials and dispersing bulk lignocellulosic materials into lignocellulosic is alkalization. Under alkaline conditions, the ester bonds in hemicelluloses and lignin are easily broken down during the alkalization. Many lignocellulosic materials have been pretreated using alkaline reagents such as NaOH, $Ca(OH)_2$, KOH, $Na_2CO_3$, and aqueous ammonia. NaOH and $Ca(OH)_2$ are the most often used alkaline reagents [24]. Further, at a temperature of 50℃, the alkalization method was performed by adding 5% NaOH. This process, also known as delignification, aimed to decrease the lignin and hemicellulose content in SCB. The amorphous component of hemicellulose might also be dissolved by NaOH, which would also turn the solution's colour dark brown. Delignification was caused by hydroxide ions ($OH^-$) from NaOH attacking the H atom linked to the phenolic OH group.

The H atom would depart as $H^+$ ions due to its partial positive charge. The basic bonds of lignin would be broken by the $OH^-$ ions of NaOH, whereas $Na^+$ ions may interact with lignin to form phenolic salts. The phenolic salt would disintegrate into the water and be thrown away during the sample washing procedure. Figure 1 illustrates the mechanism.

SCB would be alkalized before being treated with an acid hydrolysis procedure. The elimination of amorphous cellulose would make cellulose isolation easier. The addition of HCl solution with various concentrations 5, 10, 20, 25, and 30% was used to carry out this acid hydrolysis procedure. It took 12 hours to complete the acid hydrolysis process at 50℃. The hydrolysis process will accelerate with increasing HCl concentration usage, causing a large amount of glucose monomer to dissolve while washing with distilled water [25]. Following that, cellulose would be bleached. This procedure aims to increase the cellulose sample's brightness. Furthermore, one of the active bleaching agents, hypochlorite ion, destroyed the residual lignin chain and chromophore molecules throughout the bleaching process. In general, the process includes the oxidation of water-insoluble lignin to break certain bonds, including aryl ether linkages, carbon-carbon bonds, and β-O-4 bonds, and create water-soluble chemicals, including aldehydes and carboxylic acids [26]. In this study, 15% NaOCl solution with 4:1 addition of $CH_3COOH$ was used as the bleaching agent.

This study also used ultrasonication, which is effective for dispersing cellulose synthesis. Cavitation, which is caused by ultrasonic vibrations, weakens the crystal cell walls and loosens the amorphous regions. The density of the structure will be maintained if the crystal cell wall is damaged. The ultrasonic technique will promote crystallinity. The majority of the amorphous sections of cellulose are therefore hydrolyzed.

### 3.2 Compositional analysis of cellulose particles

To determine the composition of the samples, the dry weight of the samples was plotted after extractables such as ethanol and toluene soluble were removed from the samples. This is achieved by ensuring that the estimate of total cellulose content This is accomplished by making sure that the estimation of total cellulose content is independent of the sample's overall composition. Wax content is affected. Based on the results presented, the hemicellulose and lignin concentrations of samples subjected to the hydrolysis treatment phase may be found to be significantly decreased. Hemicellulose and lignin percentages in non-hydrolyzed samples were still rather high, at 27 and 36.8%, respectively. Nevertheless, the hydrolysis samples had hemicellulose and lignin percentages of 9.43% and 2.48%, respectively. It is also evident that increasing the concentration of HCl used in the hydrolysis process decreases the amount of hemicellulose and lignin while increasing the amount of α-cellulose. The contents of hemicellulose and lignin were lower in hydrolysis with 10% HCl than in hydrolysis with 5% HCl. Hemicellulose and lignin concentrations were decreased by 4.2 and 0.11%, respectively, after hydrolysis with 20% HCl. However, lignin and hemicellulose concentrations both slightly decreased after hydrolysis with HCl 25% and HCl 30%. It can be seen in Figure 2. The sample was quite black because the crystalline α-cellulose had been converted into carbon. As a result, HCl at a concentration of 20% was applied in the following stage.

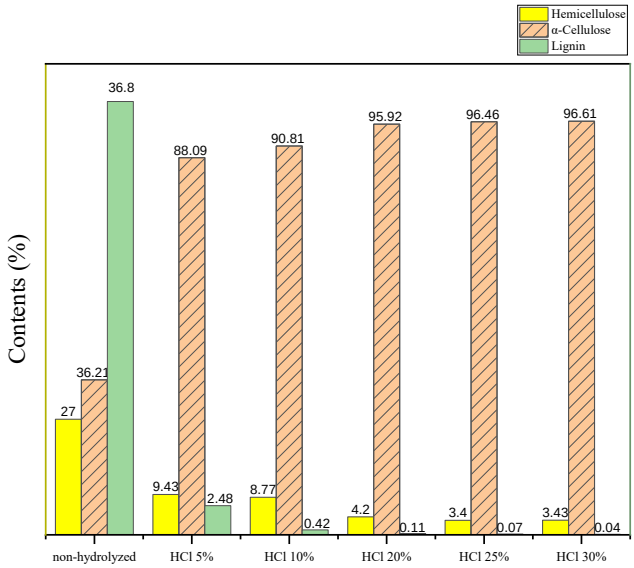


**Figure 2.** The differences in lignin, hemicellulose, and α-cellulose content in samples after different treatments

### 3.3 Characterization of cellulose particles

According to the chemical composition (hemicellulose, lignin, and α-cellulose) report, α-cellulose was efficiently generated by dewaxing, alkalization, hydrolysis, bleaching, and sonication procedures, where the concentration of HCl present also affected the percentages of hemicellulose and lignin, as well as the amount of α-cellulose that was present. It was validated by FTIR (Figure 3(a)) and XRD data (Figure 3(b)).

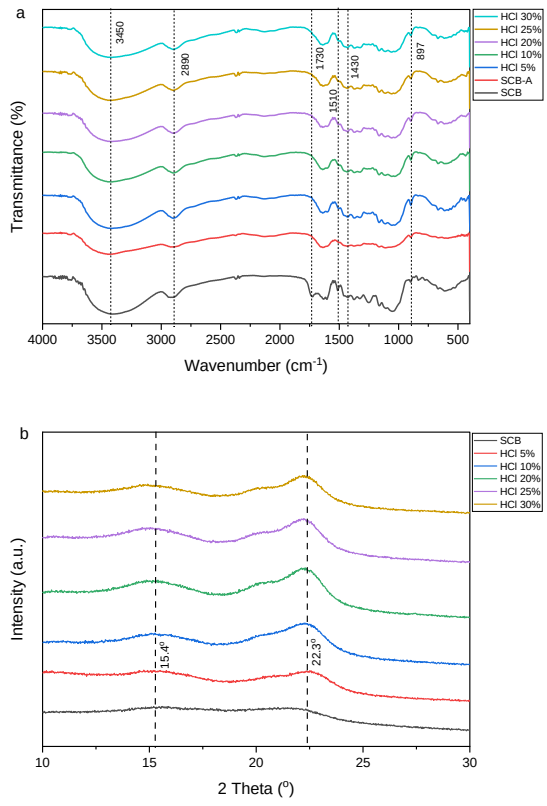


**Figure 3.** FTIR spectrum (a) and diffractograms (b) on cellulose with various hydrolysis

According to the acquired FTIR spectrum, it is evident that, with the exception of the SCB spectrum, none of the six spectra displayed the absorption band at wavenumber 1730 $cm^{-1}$ linked to stretching C=O groups in lignin and hemicellulose [27]. Similarly, after the alkalization treatment (SCB-A), the intensity of SCB in the absorption band at 1250 $cm^{-1}$ referring to the lignin's aromatic ring decreased significantly [28, 29]. Furthermore, the presence of peaks among 1510 $cm^{-1}$ wavenumber occurring in the SCB proves that lignin's methoxy groups are present and the aromatic C=C strain. The strength of the peak reduced when the material was alkalized and hydrolyzed. These findings show a considerable loss or decrease in lignin and hemicellulose content comparing SCB and SCB-A. The peak intensity of samples treated with various hydrolysis treatments (HCl 5, 10, 20, 25, and 30%) was only slightly reduced. In this situation, the HCl concentration may also be stated to have an influence on lignin and hemicellulose levels. Furthermore, the increase peak at wavenumber 897 $cm^{-1}$ was connected to cellulose stretching C-O and C-H, which resulted in greater cellulose following acid hydrolysis [17, 30]. When compared to SCB, SCB-A, HCl 5%, and HCl 10%, the intensity of the samples treated with HCl 20, 25, and 30% increased. These findings were directly related to the sample composition study, that showed more α-cellulose was produced when cellulose was hydrolyzed at higher concentrations of HCl.

In the case of cellulose I, the existence of O-H stretching on intramolecular hydrogen is shown by the absorption band at wavenumber 3175-3490 $cm^{-1}$ [19]. Furthermore, CH stretching may be seen between 2850 and 2970 $cm^{-1}$ [31]. The existence of $CH_2$ scissoring vibrations in cellulose is shown by the wavenumber 1430 $cm^{-1}$ [32]. Additionally, the crystallinity of materials containing cellulose I, cellulose II, or a mixture of the two, as well as amorphous cellulose, may be assessed using this FTIR spectral peak [33]. According to different studies for the cellulose crystal structure, the peak in the wavenumber range of 850-1500 $cm^{-1}$ is crucial. Because the spectra ratio reflects the crystallinity index, the peak at wavenumbers 1430 $cm^{-1}$ and 897 $cm^{-1}$ are highly useful in explaining the crystal structure of cellulose [31]. According to the FTIR spectra reported in this investigation, hydrolysis enhanced the intensity at wavenumbers 1430 $cm^{-1}$ and 897 $cm^{-1}$. The peak more sharply in the HCl 10% and HCl 20%. However, the strength of the HCl 25% and HCl 30% samples decreased somewhat. These findings show that the hydrolysis process can remove the amorphous structure of cellulose, resulting in a greater crystalline cellulose concentration in the sample. In relation to the outcomes produced by XRD, these findings are equally relevant.

XRD has an advantage over other crystallinity measurement methods since the collected data is more accurate [34]. When X-rays are diffracted, the crystalline component of cellulose emits a significant signal. According to Ferreira et al. [35], it is possible to determine crystallographic characteristics in this situation, including crystal unit cell separation. Following the hydrolysis process, the sample's crystallinity index improved; the crystallinity index grew inversely with HCl concentration. The equation may be used to determine the crystallinity index (Eq. (8)) [36]:

$$\frac{Crystalline\ peak\ area}{Total\ area\ of\ all\ Peak\ (crystalline+amorphous)} \text{ x } 100 \qquad (8)$$

In cellulose particles, the crystalline peak region is located at angles of 2θ = 15.4˚ and 22.3˚. This is also consistent with Kumar et al. [31] and Park et al. [37]. In each sample that has undergone the hydrolysis procedure, the diffractogram (Figure 3(b)) reveals peak intensity increases at an angle of 2 = 22.3˚. The drop in peak intensity, on the other hand, occurs at an angle of 2θ = 18˚, representing cellulose amorphous. In this investigation, the Scherrer equation was used to determine the sample's crystalline size (Eq. (9)) [12]:

$$D = \frac{K\lambda}{\beta_{1/2}\, cos\theta} \qquad (9)$$

D, K, λ, θ and β are size of crystalline (nm), Scherrer constant (0.91), radiation wavelength (1.54060 nm), the diffraction angle, and FWHM (radians) respectively.

The data from each sample's estimated crystallinity index and crystalline size are shown in Figure 4. On the basis of these calculations, it can be shown that cellulose's crystallinity index and crystalline size were both impacted by the HCl concentration used to hydrolyze cellulose. The crystallinity index increased significantly at HCl concentrations ranging from 5 to 20%. The acid used during hydrolysis caused an increase in the crystallinity index. As soon as the cellulose's amorphous component broke down, the crystalline part was formed. Acid degrades the amorphous cellulose chain more easily than the crystalline cellulose chain [38].

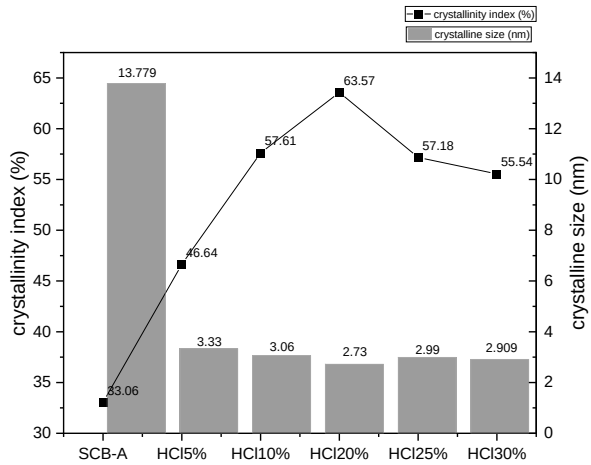


**Figure 4.** The crystalline size and crystallinity index of cellulose with various treatments

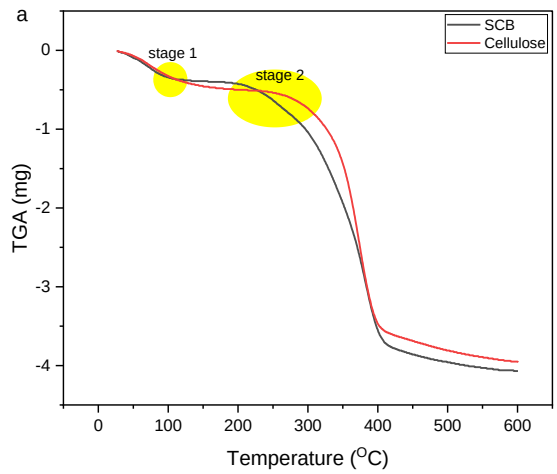


**Figure 5.** Thermograms of SCB and cellulose particles

The cellulose crystallinity index is an essential feature of cellulose because it influences its mechanical and physical characteristics. The physical and mechanical characteristics of cellulose particles with a high crystallinity index are excellent. This is due to hydrogen bonds between cellulose chains and Van der Waals interactions between glucose molecules forming the crystalline structure of cellulose. The degree of cellulose crystallinity also influences the efficacy of the hydrolysis process. As a result, knowing cellulose crystallinity index is critical before proceeding with additional processing in order to optimize the chemicals utilized, manufacturing, and analysis time.

A TGA curve depicts the sample's weight loss in 2 stages. The first stage at 75-150℃ is associated with weight loss in the sample as a result of absorbed moisture evaporation. A second weight loss is recorded in the range of temperature 360-575℃ owing to complete degradation to ash. Cellulose particles have the lowest residue since it has the fewest contaminants. Following treatments, cellulose's thermal resistance increased (Figure 5). The maximal disintegration rate for SCB was 318℃, which was changed to 333℃ for cellulose particles. This temperature change is caused by the highly density cellulose particles caused by high intermolecular hydrogen bonding [19].

### 3.4 Adsorption study

The cationic dye methylene blue has positively charged surface groups. As a result of electrostatic attraction, It may be adsorbed by any adsorbent with exposed anionic functional groups. Furthermore, as shown subsequently, the hydroxyl on the cellulose surfaces may play an essential part of the adsorption mechanism. This study also investigated important factors in the methylene blue adsorption process such as effect of contact time and pH adsorption, adsorption isotherm and adsorption kinetic.

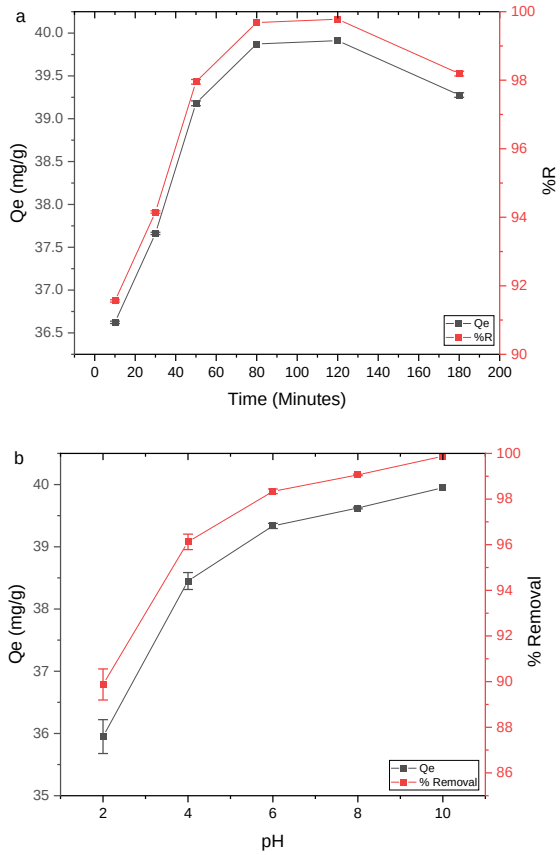


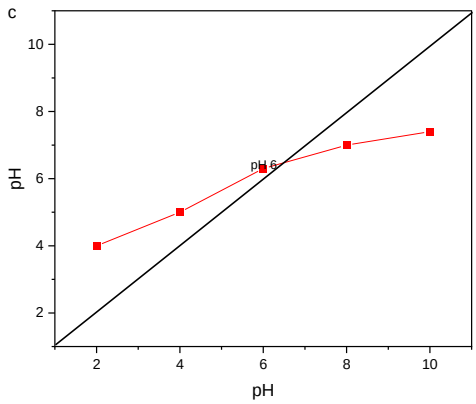


**Figure 6.** The impact of contact time

*a) Adsorption parameters*

Cellulose particles were used to establish the optimum contact time and pH for MB adsorption. Figure 6(a) shows the results of the optimal contact time in the adsorption processes. Based on the data, there is an enhancement in adsorption capacity and % removal of MB from 10 to 120 minutes. Adsorption increases with longer contact duration until it reaches equilibrium. There were a lot of unused active sites in the adsorbent during the beginning contact times. When the removal rate is slow, adsorbate diffusion, which is physical rather than chemical, occurs [22]. After 120 minutes of contact time, equilibrium was reached as demonstrated by maximum in adsorption capacity (39.91 mg/g). The term "equilibrium" refers to the condition that the amount of MB desorbed and adsorbed is identical. As a result, 120 minutes of contact time was chosen as the optimum contact time for further investigation.

(b) and pH (a) on adsorption performance, also $pH_{pzc}$ data (c). $pH_{pzc}$ was determined by subtracting the pH drift technique was used to calculate the starting pH (black line) and final pH (red line) (0.1 M $KNO_3$, 72 h). pH is equally important as contact time. The change in adsorption capacity at various pH values of the solution can be used to study this. The effect of pH on MB adsorption onto cellulose can be seen in Figure 6(b). To improve MB adsorption, it is necessary to manage the system's pH. When pH was increased from 1 to 10, the percentage of MB removal increased from approximately 89-99.87% and the adsorption capacity improved from around 35-39.95 mg/g. Electrical property changes caused by pH can explain this effect of the MB and cellulose particles. Under strongly acidic [18] circumstances, the hydroxyl groups in the cellulose will have been protonated, decreasing their ability to attract cationic MB molecules. This reduces the adsorption capability. The hydroxyl groups have been deprotonated, which has caused them to have negative charges at higher pH levels. As a result, they may bind the positively charged MB molecules at these higher pH levels. To validate this, we used the pH drift method to determine the point of zero charge ($pH_{pzc}$) (Figure 6(c)). $pH_{pzc}$ of cellulose was 6. Cellulose surface was predicted to be positive if the solution's pH was lower than $pH_{pzc}$. Electrostatic attraction was usually attributed to MB adsorption by cellulose. Thus, adsorbate containing the same positive charge with adsorbent might be electrostatically repulsed. It could decrease the adsorption capability.

*b) Adsorption isotherm study*

To represent the equilibrium of adsorption, adsorption isotherms were employed. The adsorption isotherm explains how the adsorbent interacts with MB and its adsorption

properties. The foundation of the Langmuir equation is the concept that adhesion to an adsorbent surface causes a homogeneous monolayer of adsorbate to form. However, the Freundlich equation presupposes since each binding site has a different amount of energy, leading to heterogeneity and potentially multilayer adsorption. Figure 7(a) shows the Langmuir and Freundlich curves for adsorption isotherms. The comparison of modified $R^2$ values based on the curve obtained further reveals that cellulose particles during the adsorption process conform to the Freundlich isotherm model. The $K_f$ for MB adsorption onto cellulose particles was 66.386 mg/g.

*c) Adsorption kinetic study*

Pseudo-first-order (PFO) and pseudo-second-order (PSO) kinetic models were used to study the adsorption kinetics of MB onto the cellulose particles. The pseudo first order and pseudo second order models' non-linear adsorption kinetics equations are presented in Figure 7(b). The maximum adsorption capacity for the pseudo second order in this case is 39.969 mg/g, and the adsorption kinetics generally follow this model. A pseudo-second order adsorption rate constant (k2) of 0.0276 g/mg.min was measured. With an $R^2$ value close to 1, the pseudo second order model explained the data more effectively. It can be seen in the Table 1. Based on the data, it can be concluded that the adsorbate and adsorbent's ability to transport electrons controlled how much methylene blue was removed [39].

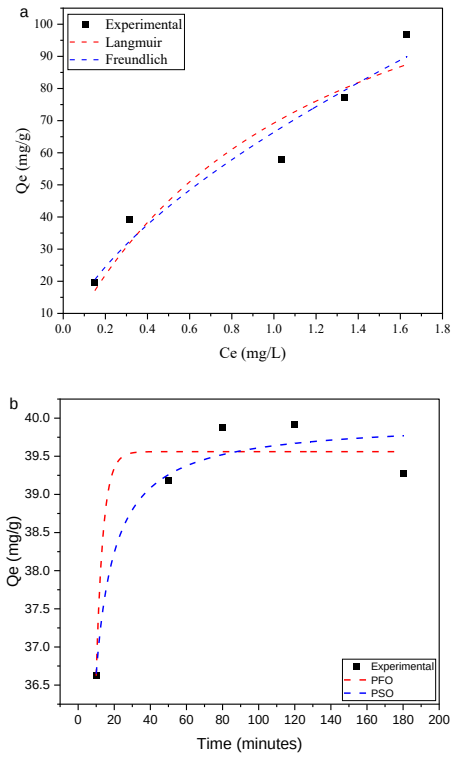


**Figure 7.** Non-linear isotherm models (a) and kinetic models for MB adsorption onto cellulose particles (b)

**Table 1.** Isotherm and kinetic parameters for MB adsorption onto cellulose

| | Models | Equation | Parameters | Value |
|---|---|---|---|---|
| **Isotherm** | Langmuir | $Q_e = \frac{Q_{max}.K_L.C_e}{1+K_L.C_e}$ | Adjusted $R^2$ | 0.885 |
| | | | $K_L$ (L/mg) | 0.856 |
| | | | Qmax (mg/g) | 150.06 |
| | Freundlich | $Q_e = K_F.C_e^{\frac{1}{n}}$ | Adjusted $R^2$ | 0.928 |
| | | | $K_F$ (mg/g) | 66.36 |
| | | | n | 0.697 |
| **Kinetic** | Pseudo-First-Order (PFO) | $q_t = Q_e(1-e^{k_1 t})$ | Adjusted $R^2$ | 0.919 |
| | | | $K_1$ (g/mg.min) | 0.260 |
| | | | Qe (mg/g) | 39.58 |
| | Pseudo-Second-Order (PSO) | $q_t = \frac{Q_e^2 k_2 t}{1+q_t k_2 t}$ | Adjusted $R^2$ | 0.921 |
| | | | $K_2$ (g/mg.min) | 0.027 |
| | | | Qe (mg/g) | 39.96 |

in which, Qe stands for the amount of MB adsorbed at equilibrium (mg/g), Ce for the concentration of MB at equilibrium (mg/L), Qmax for the maximum adsorption capacity (mg/g), and KL for the Langmuir constant (L/mg). KF: adsorption capacity (mg/g), 1/n: system adsorption intensity. qt is the quantity of MB that cellulose particles have adsorbed at equilibrium at time t (in mg/g), $k_1$ is the PFO rate constant (1/min), $k_2$ is the PSO rate constant (in mg/mg min); and t is the time.

*d. Adsorption mechanism*

FT-IR study on the cellulose particles before and after adsorption was used to investigate the effect of the functional group during MB adsorption (Figure 8). Several differences in the FT-IR spectrum profile following MB adsorption are attributed to disturbances in the vibration of N-H, C=O, and O-H. Functional groups containing O and N have been attributed to the removal of a wide range of pollutants. Adsorption mechanism studies indicated the importance of functional groups in establishing electrostatic attraction with the adsorbate. When the cellulose particles spectra were compared before and after treatment, it was discovered that the majority of the absorption bands had been moved to lower frequencies. These changes were consistent with previous reports of cellulose treatment [40, 41]. This data is also supported by several other studies, which also prove that an important role in an adsorption process is the functional group contained in the adsorbent [42-44].

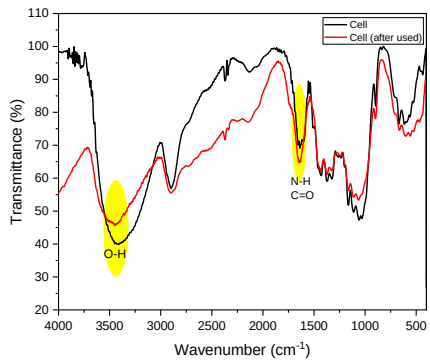


**Figure 8.** Comparison of spectra before and after MB adsorption on cellulose

## 4. CONCLUSIONS

This study was successful in isolating cellulose particles from sugarcane bagasse. In case of composition of the sample, SCB that had been hydrolyzed with 20% HCl included more α-cellulose and less lignin and hemicellulose. The crystallinity index of the cellulose particles produced in this study was 63.57%, and their average crystalline size was 2.73 nm. Adsorption studies also demonstrated that cellulose particles from sugarcane bagasse was particularly effective in methylene blue adsorption. According to spectroscopic results, the C-OH, C=O, C-O, and OH groups were mainly significant for MB dye adsorption. Cellulose particles have a high maximum adsorption capacity of MB (66.386 mg/g). The high maximum adsorption capacity achieved on sugarcane bagasse-derived cellulose is evidence that it can be used to treat textile industry waste containing cationic dyes. As a result, this research was successful in converting sugarcane bagasse, which is categorized as waste and has no value, into a product with a high value in order to address environmental contamination caused by textile industry waste, which is now prevalent. The cellulose produced in this study has several advantages over previous studies, including a high crystallinity index, superior heat resistance, and application in methylene blue removal. In this paper, we detail each treatment procedure used to obtained cellulose particles. In order to be a source of information in future studies, we also detail the process for lignocellulose breakdown, the reaction mechanism between cellulose and methylene blue, and study at adsorption experiments.


## ACKNOWLEDGEMENTS

The authors were grateful to Universitas Syiah Kuala for providing funding under Grant Number: 487/UN11/SPK/PNBP/2022 under PRUUPD program. The authors were also grateful to those who provided suggestions when preparing this work.


## THE CONTRIBUTIONS OF AUTHORS

All authors participated in conception and design of the study. Haya Fathana, Rahmi, Muhammad Adlim, Surya Lubis, and Muhammad Iqhramullah prepared the materials and collected the data. The manuscript's first draft was written by Haya Fathana, and subsequent drafts were revised with input from various authors. All writers evaluated and approved the final text.

## REFERENCES


[1] Yang, S.L., Zhang, Y.B., Deng, J., Li, R.D., Fan, X., Dao, J.M., Quan, Y.J., Bukhari, S.A.H. (2021). Effect of cutting depth during sugarcane (Saccharum spp. hybrid) harvest on root characteristics and yield. PLoS One, 16(1): e0238085. https://doi.org/10.1371/journal.pone.0238085

[2] Dotaniya, M.L., Datta, S.C., Biswas, D.R., Dotaniya, C.K., Meena, B.L., Rajendiran, S., Regar, K.L., Lata, M. (2016). Use of sugarcane industrial by-products for improving sugarcane productivity and soil health. International Journal of Recycling of Organic Waste in Agriculture, 5(3): 185-194. https://doi.org/10.1007/s40093-016-0132-8

[3] Evans, S.K., Wesley, O.N., Nathan, O., Moloto, M.J. (2019). Chemically purified cellulose and its nanocrystals from sugarcane baggase: Isolation and characterization. Heliyon, 5(10): e02635. https://doi.org/10.1016/j.heliyon.2019.e02635

[4] Anukam, A., Mamphweli, S., Reddy, P., Meyer, E., Okoh, O. (2016). Pre-processing of sugarcane bagasse for gasification in a downdraft biomass gasifier system: A comprehensive review. Renewable and Sustainable Energy Reviews, 66: 775-801. https://doi.org/10.1016/j.rser.2016.08.046

[5] Sukyai, P., Anongjanya, P., Bunyahwuthakul, N., Kongsin, K., Harnkarnsujarit, N., Sukatta, U., Sothornvit, R., Chollakup, R. (2018). Effect of cellulose nanocrystals from sugarcane bagasse on whey protein isolate-based films. Food Research International, 107: 528-535. https://doi.org/10.1016/j.foodres.2018.02.052

[6] Mohammed, N., Lian, H., Islam, M.S., Strong, M., Shi, Z.Q., Berry, R.M., Yu, H.Y., Tam, K.C. (2021). Selective adsorption and separation of organic dyes using functionalized cellulose nanocrystals. Chemical Engineering Journal, 417: 129237. https://doi.org/10.1016/j.cej.2021.129237

[7] Georgouvelas, D., Abdelhamid, H.N., Li, J., Edlund, U., Mathew, A.P. (2021). All-cellulose functional membranes for water treatment: Adsorption of metal ions and catalytic decolorization of dyes. Carbohydrate Polymers, 264: 118044. https://doi.org/10.1016/j.carbpol.2021.118044

[8] Sayyed, A.J., Pinjari, D.V., Sonawane, S.H., Bhanvase, B.A., Sheikh, J., Sillanpää, M. (2021). Cellulose-based nanomaterials for water and wastewater treatments: A review. Journal of Environmental Chemical Engineering, 9(6): 106626. https://doi.org/10.1016/j.jece.2021.106626

[9] Wang, D. (2019). A critical review of cellulose-based nanomaterials for water purification in industrial processes. Cellulose, 26(2): 687-701. https://doi.org/10.1007/s10570-018-2143-2

[10] Marques, G., Rencoret, J., Gutiérrez, A., del Río, J.C. (2020). Lipophilic compounds from maize fiber and rice husk residues – An abundant and inexpensive source of valuable phytochemicals. Industrial Crops and Products, 146: 112203. https://doi.org/10.1016/j.indcrop.2020.112203

[11] Paulraj Gundupalli, M., Cheng, Y.S., Chuetor, S., Bhattacharyya, D., Sriariyanun, M. (2021). Effect of dewaxing on saccharification and ethanol production from different lignocellulosic biomass. Bioresource Technology, 339: 125596. https://doi.org/10.1016/j.biortech.2021.125596

[12] Lin, Q., Huang, Y., Yu, W. (2021). Effects of extraction methods on morphology, structure and properties of bamboo cellulose. Industrial Crops and Products, 169: 113640. https://doi.org/10.1016/j.indcrop.2021.113640

[13] Norizan, M.N., Shazleen, S.S., Alias, A.H. (2022). Nanocellulose-based nanocomposites for sustainable applications: A review. Nanomaterials, 12(19): 1-51. https://doi.org/10.3390/nano12193483

[14] Sri Aprilia, N.A., Mulyati, S., Alam, P.N., Razali, Zuhra, N., Fatmawati, Kamaruzaman, S., Amin, A. (2021).

Preparation and characterization of sugarcane bagasse nanocellulose crystalline using acid hydrolysis with and without ultrasonication. Rasayan J. Chem., 14(1): 601-607. https://doi.org/10.31788/RJC.2021.1415920

[15] Abitbol, T., Rivkin, A., Cao, Y.F., Nevo, Y., Abraham, E., Ben-Shalom, T., Lapidot, S., Shoseyov, O. (2016). Nanocellulose, a tiny fiber with huge applications. Current Opinion in Biotechnology, 39(1): 76-88. https://doi.org/10.1016/j.copbio.2016.01.002

[16] de Oliveira, F.B., Bras, J., Pimenta, M.T.B., da Silva Curvelo, A.A., Belgacem, M.N. (2016). Production of cellulose nanocrystals from sugarcane bagasse fibers and pith. Industrial Crops and Products, 93: 48-57. https://doi.org/10.1016/j.indcrop.2016.04.064

[17] Yin, Y., Ma, J., Tian, X., Jiang, X., Wang, H., Gao, W. (2018). Cellulose nanocrystals functionalized with amino-silane and epoxy-poly(ethylene glycol) for reinforcement and flexibilization of poly(lactic acid): Material preparation and compatibility mechanism. Cellulose, 25(11): 6447-6463. https://doi.org/10.1007/s10570-018-2033-7

[18] Hosseini, H., Zirakjou, A., McClements, D.J., Goodarzi, V., Chen, W.H. (2022). Removal of methylene blue from wastewater using ternary nanocomposite aerogel systems: Carboxymethyl cellulose grafted by polyacrylic acid and decorated with graphene oxide. Journal of Hazardous Materials, 421: 126752. https://doi.org/10.1016/j.jhazmat.2021.126752

[19] Abral, H., Ariksa, J., Mahardika, M., Handayani, D., Aminah, I., Sandrawati, N., Pratama, A.B., Fajri, N., Sapuan, S.M., Ilyas, R.A. (2020). Transparent and antimicrobial cellulose film from ginger nanofiber. Food Hydrocolloids, 98: 105266. https://doi.org/10.1016/j.foodhyd.2019.105266

[20] Demsash, E.G.H.D. (2021). Extraction and Characterization of Nanocellulose from Eragrostis Teff Straw. J. Cellul. https://www.researchsquare.com/article/rs-296990/latest.pdf.

[21] ZabihiSahebi, A., Koushkbaghi, S., Pishnamazi, M., Askari, A., Khosravi, R., Irani, M. (2019). Synthesis of cellulose acetate/chitosan/SWCNT/$Fe_3O_4$/$TiO_2$ composite nanofibers for the removal of Cr(VI), As(V), Methylene blue and Congo red from aqueous solutions. International Journal of Biological Macromolecules, 140: 1296-1304. https://doi.org/10.1016/j.ijbiomac.2019.08.214

[22] Marlina, Iqhrammullah, M., Darmadi, Mustafa, I., Rahmi. (2019). The application of chitosan modified polyurethane foam adsorbent. Rasayan J. Chem., 12(2): 494-501. https://doi.org/10.31788/RJC.2019.1225080

[23] Marrakchi, F., Khanday, W.A., Asif, M., Hameed, B.H. (2016). Cross-linked chitosan/sepiolite composite for the adsorption of methylene blue and reactive orange 16. Int. J. Biol. Macromol., 93: 1231-1239. https://doi.org/10.1016/j.ijbiomac.2016.09.069

[24] Sun, S., Sun, S., Cao, X., Sun, R. (2016). The role of pretreatment in improving the enzymatic hydrolysis of lignocellulosic materials. Bioresource Technology, 199: 49-58. https://doi.org/10.1016/j.biortech.2015.08.061

[25] Effendi, F., Elvia, R., Amir, H. (2018). Preparasi dan karakterisasi mikrokristalin selulosa (Mcc) berbahan baku tandan kosong kelapa sawit (Tkks). Alotrop, 2(1): 52-57. https://doi.org/10.33369/atp.v2i1.4672

[26] Wang, T., Zhao, Y. (2021). Optimization of bleaching process for cellulose extraction from apple and kale pomace and evaluation of their potentials as film forming materials. Carbohydrate Polymers, 253: 117225. https://doi.org/10.1016/j.carbpol.2020.117225

[27] Zhao, Y., Moser, C., Lindström, M.E., Henriksson, G., Li, J. (2017). Cellulose nanofibers from softwood, hardwood, and tunicate: Preparation-structure-film performance interrelation. ACS Appl. Mater. Interfaces, 9(15): 13508-13519. https://doi.org/10.1021/acsami.7b01738

[28] Carneiro de Oliveira, J., Rigolet, S., Marichal, C., Roucoules, V., Laborie, M.P. (2020). Grafting Diels-Alder moieties on cellulose nanocrystals through carbamation. Carbohydrate Polymers, 250: 116966. https://doi.org/10.1016/j.carbpol.2020.116966

[29] Huang, B., He, H., Liu, H., Zhang, Y., Peng, X., Wang, B. (2020). Multi-type cellulose nanocrystals from sugarcane bagasse and their nanohybrids constructed with polyhedral oligomeric silsesquioxane. Carbohydrate Polymers, 227: 115368. https://doi.org/10.1016/j.carbpol.2019.115368

[30] Huang, X., Xie, F., Xiong, X. (2018). Surface-modified microcrystalline cellulose for reinforcement of chitosan film. Carbohydrate Polymers, 201: 367-373. https://doi.org/10.1016/j.carbpol.2018.08.085

[31] Kumar, A., Singh Negi, Y., Choudhary, V., Kant Bhardwaj, N. (2020). Characterization of cellulose nanocrystals produced by acid-hydrolysis from sugarcane bagasse as agro-waste. Journal of Materials Physics and Chemistry, 2(1): 1-8. https://doi.org/10.12691/jmpc-2-1-1

[32] Ni, H., Zeng, S.Q., Wu, J., Cheng, X.R. (2012). Cellulose nanowhiskers: Preparation, characterization and cytotoxicity evaluation. Biomed. Mater. Eng., 22(1-3): 121-127. https://doi.org/10.3233/BME-2012-0697

[33] Carrillo, F., Colom, X., Suñol, J.J., Saurina, J. (2004). Structural FTIR analysis and thermal characterisation of lyocell and viscose-type fibres. European Polymer Journal, 40(9): 2229-2234. https://doi.org/10.1016/j.eurpolymj.2004.05.003

[34] Kedzior, S.A., Zoppe, J.O., Berry, R.M., Cranston, E.D. (2019). Recent advances and an industrial perspective of cellulose nanocrystal functionalization through polymer grafting. Current Opinion in Solid State and Materials Science, 23(2): 74-91. https://doi.org/10.1016/j.cossms.2018.11.005

[35] Ferreira, F.V., Dufresne, A., Pinheiro, I.F., Souza, D.H.S., Gouveia, R.F., Mei, L.H.I., Lona, L.M.F. (2018). How do cellulose nanocrystals affect the overall properties of biodegradable polymer nanocomposites: A comprehensive review. European Polymer Journal, 108: 274-285. https://doi.org/10.1016/j.eurpolymj.2018.08.045

[36] Lopes, I.S., Michelon, M., Duarte, L.G.R., Prediger, P., Cunha, R.L., Picone C.S.F. (2021). Effect of chitosan structure modification and complexation to whey protein isolate on oil/water interface stabilization. Chemical Engineering Science, 230: 116124. https://doi.org/10.1016/j.ces.2020.116124

[37] Park, S.H., Shin, S.S., Park, C.H., Jeon, S., Gwon, J., Lee, S.Y., Kim, S.J., Kim, H.J., Lee, J.H. (2020). Poly(acryloyl hydrazide)-grafted cellulose nanocrystal adsorbents with an excellent Cr(VI) adsorption capacity.

Journal of Hazardous Materials, 394: 122512. https://doi.org/10.1016/j.jhazmat.2020.122512
[38] Siti, A. (2018). Penentuan Derajat Kristalinitas Selulosa, α-Selulosa, Dan Mikrokristal Selulosa (MKS) Dari Daun Gebang (Corypha utan Lamk). pp. 1-63. http://repositori.usu.ac.id/handle/123456789/6669.
[39] Ismail, B., Hussain, S.T., Akram, S. (2013). Adsorption of methylene blue onto spinel magnesium aluminate nanoparticles: Adsorption isotherms, kinetic and thermodynamic studies. Chemical Engineering Journal, 219: 395-402. https://doi.org/10.1016/j.cej.2013.01.034
[40] Al-Mokhalelati, K., Al-Bakri, I., Al Shibeh Al Wattar, N. (2021). Adsorption of methylene blue onto sugarcane bagasse-based adsorbent materials. J. Phys. Org. Chem., 34(7): 1-9. https://doi.org/10.1002/poc.4193
[41] Chowdhury, S., Das Saha, P. (2012). Biosorption of methylene blue from aqueous solutions by a waste biomaterial: Hen feathers. Applied Water Science, 2(3): 209-219. https://doi.org/10.1007/s13201-012-0039-0
[42] Rahmi, Julinawati, Nina, M., Fathana, H., Iqhrammullah, M. (2022). Preparation and characterization of new magnetic chitosan-glycine-PEGDE ($Fe_3O_4$/Ch-G-P) beads for aqueous Cd(II) removal. Journal of Water Process Engineering, 45: 102493. https://doi.org/10.1016/j.jwpe.2021.102493
[43] Nikiforova, T.E., Kozlov, V.A., Telegin, F.Y. (2021). Chemisorption of copper ions in aqueous acidic solutions by modified chitosan. Materials Science and Engineering: B, 263: 114778. https://doi.org/10.1016/j.mseb.2020.114778
[44] Abdul Khalil, H.P.S., Saurabh, C.K., Adnan, A.S., Nurul Fazita, M.R., Syakir, M.I., Davoudpour, Y., Rafatullah, M., Abdullah, C.K., Haafiz, M.K.M. Dungani, R. (2016). A review on chitosan-cellulose blends and nanocellulose reinforced chitosan biocomposites: Properties and their applications. Carbohydrate Polymers, 150: 216-226. https://doi.org/10.1016/j.carbpol.2016.05.028